

Strain-based seismic failure evaluation of coupled dam-reservoir-foundation system

M.A. Hariri-Ardebili^{*1}, H. Mirzabozorg² and A. Ghasemi²

¹*Department of Civil Environmental and Architectural Engineering, University of Colorado at Boulder, P.O. Box 80309-0428, Boulder, CO, USA*

²*Department of Civil Engineering, K. N. Toosi University of Technology, P.O. Box 15875-4416, Tehran, Iran*

(Received January 27, 2013, Revised March 3, 2013, Accepted March 10, 2013)

Abstract. Generally, mass concrete structural behavior is governed by the strain components. However, relevant guidelines in dam engineering evaluate the structural behavior of concrete dams using stress-based criteria. In the present study, strain-based criteria are proposed for the first time in a professional manner and their applicability in seismic failure evaluation of an arch dam are investigated. Numerical model of the dam is provided using NSAD-DRI finite element code and the foundation is modeled to be massed using infinite elements at its far-end boundaries. The coupled dam-reservoir-foundation system is solved in Lagrangian-Eulerian domain using Newmark- β time integration method. Seismic performance of the dam is investigated using parameters such as the demand-capacity ratio, the cumulative inelastic duration and the extension of the overstressed/overstrained areas. Real crack profile of the dam based on the damage mechanics approach is compared with those obtained from stress-based and strain-based approaches. It is found that using stress-based criteria leads to conservative results for arch action while seismic safety evaluation using the proposed strain-based criteria leads to conservative cantilever action.

Keywords: dam-foundation interaction; massed foundation; strain-based criteria; damage mechanics; infinite elements

1. Introduction

Engineers should pay special attention to the problem of earthquake loading in design and evaluation of the concrete arch dams. Performance of arch dams maybe evaluated in linear or nonlinear phases considering different assumptions for material and loading. First, it is common to evaluate the seismic behavior in the linear domain. In the case of extensive stresses in the dam body, nonlinear analysis should be implemented.

Several researchers have investigated seismic performance of concrete arch dams such as; Chopra (1998), Hall *et al.* (1999), Ghanaat (2004), Bayraktar *et al.* (2009), and Hariri-Ardebili *et al.* (2011). Ghanaat (2004) proposed a methodology for damage estimation in concrete dams which can be found in US Army Corps of Engineers (*USACE*) guideline (2007) and used these criteria for assessment of *Morrow point* and *Pacioma* arch dams. Bayraktar *et al.* (2009) evaluated seismic performance of the concrete gravity, arch, RCC and CFRD dams using indices proposed

*Corresponding author, Ph.D. Research Assistant, E-mail: mohammad.haririardabili@colorado.edu

by *USACE* subjecting to near- and far-fault ground motions. Hariri-Ardebili *et al.* (2011) investigated the effect of water level on dynamic performance of arch dams. They found that dewatering the reservoir can lead to extension of the overstressed area on upstream and downstream faces. Hariri-Ardebili and Mirzabozorg (2011) studied seismic performance of concrete arch dams subjected to real ground motions and also Endurance Time Acceleration Functions (*ETAFs*) using *USACE* indices. Some other researchers were investigated performance of specific dams or used stochastic methods in order to evaluate seismic performance of concrete dams such as; Wieland *et al.* (2003), Studer (2004), Yamaguchi *et al.* (2004), and Hariri-Ardebili *et al.* (2012).

On the other hand, some researchers used the methods based on damage mechanics and combination of this method with the theory of plasticity, discrete crack approach and other techniques in order to simulation of the cracking and failure in concrete dams such as, Horii and Chen (2003), Calayir and Karaton (2005), Ardakanian *et al.* (2006), Oliveira and Faria (2006), and Papadrakakis *et al.* (2008). Pan *et al.* (2011) compared the different procedures for seismic cracking analysis of concrete arch and gravity dams. Omidi *et al.* (2013) studied the seismic cracking behavior of concrete gravity dams using plastic-damage model considering different damping mechanisms. Zhang *et al.* (2013) investigated the effects of the strong motion duration on the nonlinear dynamic response of concrete gravity dams using damage plasticity model.

All the previous researches are limited to use of the stress as a factor to determine the seismic behavior of concrete dams. In most cases parameters like as demand-capacity ratio (*DCR*) is calculated based on the stress time-history of the most critical point of the dam. However, it's important to note that the behavior of concrete especially in cracking is based on the strain variation. It means that concrete fails when its strain exceeds a predefined value called ultimate strain. So in the present paper, common criteria for seismic assessment of concrete arch dams based on stress are substituted by similar criteria, which act based on the strain. The results were compared using *DCR*, cumulative inelastic duration (*CID*) and percentage of the overstressed or overstrained area within the dam body for various load combinations. In addition nonlinear analysis of the dam is performed using the damage mechanics approach in order to figure out the real crack profile and compare the results with those estimated from linear method.

2. Seismic performance evaluation

Generally, safety and serviceability of large mass concrete structures is controlled by the tensile behavior of material. Actual response of the massive concrete structures to the earthquake ground motions is too complicated. Loading histories and rapid seismic strain rates have an important role on structural performance (*USACE* 2007). As it is known, mass concrete has limited ductile behavior. This behavior is characterized by a stress-strain relation composed of elastic and inelastic strain ranges followed by a complete loss of strength (*USACE* 2007). The tensile stress-strain diagram of mass concrete is shown in Fig. 1. As can be seen, the curve is divided into the three parts. In the first section, in which the concrete behaves as a linear elastic (*LE*) material, the dam is called to have serviceability performance. The second part is inelastic-strain hardening range known as damage control range and causes only limited inelastic behavior in the dam body. In this situation damage may be significant but all cracking and joint openings are limited and discrete (Ghanaat 2004). Except for unlikely Maximum Credible Level (*MCL*) events, it is desired to prevent damage in the main elements such as foundation and other inaccessible affecting

elements. A LE analysis combined with a predefined performance evaluation criteria can be used to investigate the dam response in the damage control range. The dam response beyond the damage control range is called collapse prevention performance and must be evaluated using nonlinear time-history analysis.

Fig.2 describes the general methodology for the seismic evaluation of concrete arch dams using stress-based or strain-based criteria. Seismic performance of concrete arch dams is evaluated using displacements, stresses, *DCR*, *CID* and spatial extension of overstressed (or overstrained) areas on the upstream (*US*) and downstream (*DS*) faces of the dam body

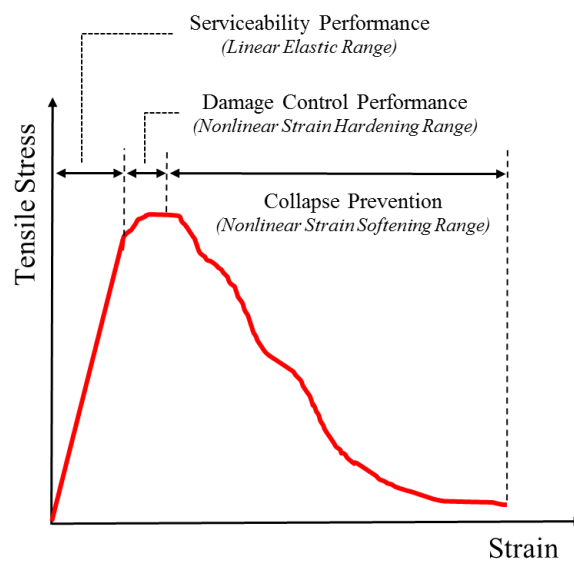


Fig. 1 Conventional stress-strain relation for mass concrete structures (USACE 2007)

2.1. Demand capacity ratio

For the arch dams where affecting stresses and strains usually oriented in the arch and cantilever directions, *DCR* refers to the ratio of the calculated arch or cantilever stress or strain to the tensile strength of mass concrete or its equivalent strain, but it can also be developed for principal stresses (or strains) (Ghanaat 2004). Tensile strength of mass concrete used for computing *DCR* is obtained from uniaxial splitting tension tests or from Raphael (1984) proposed diagram, while the equivalent strain is calculated using Hock's law in static condition. The maximum permitted *DCR* for linear analysis of dams using stress-based rule is 2.0. This corresponds to a stress demand twice the tensile strength of mass concrete. So the *DCR* can be summarized as Eqs. (1) and (2) for stress and strain, respectively

$$\left\{ \begin{array}{l} DCR_{stress}^{arch} = \frac{\text{arch stress demand}}{\text{tensile strength}} = \frac{\sigma^{arch}}{f_t'} \\ DCR_{stress}^{cantil} = \frac{\text{cantilever stress demand}}{\text{tensile strength}} = \frac{\sigma^{contl}}{f_t'} \end{array} \right. \quad (1)$$

$$\left\{ \begin{array}{l} DCR_{stress}^{arch} = \frac{\text{arch strain demand}}{\text{static tensile strain}} = \frac{\varepsilon^{arch}}{f_t'/E_c} \\ DCR_{stress}^{cantil} = \frac{\text{cantilever strain demand}}{\text{static tensile strain}} = \frac{\varepsilon^{contl}}{f_t'/E_c} \end{array} \right. \quad (2)$$

where f_t' and E_c are tensile strength and modulus of elasticity of mass concrete, respectively.

2.2. Cumulative inelastic duration

Cumulative inelastic duration, which is a measure of energy, accounts for magnitudes as well as duration of the stress (or strain) excursions. It refers to the total duration of stress or strain excursions above a stress (or strain) level associated with a certain *DCR* (USACE 2007). The higher cumulative duration, the higher is the probability for more damage. For assessing the level of damage, *CID* is utilized in conjunction with *DCR*. The authors use the methodology of *USACE* for evaluation of the arch dams' performance using *LE* analyses. In this method the behavior of the dam is evaluated in three zones based on the estimated damage severity. Performance Threshold Curve (*PTC*) for arch dams is shown in Fig. 3.

2.3. Spatial extension of overstressed (or overstrained) areas

In addition to foregoing performance criteria, the introduced damage criteria require to be bounded in limited areas, so that evaluation based on *LE* analysis is still valid. If spatial extension of damage or nonlinear response is limited to 20% of total areas on the upstream or downstream faces, *LE* analysis is valid (USACE 2007).

2.4. Quantitate of limit-states

Herein, the *USACE* methodology is introduced to quantify the pointed out limit-states (*LS*) in above subsections. In fact, this methodology extends the qualify concept of limit states to quantitative values, as described in Table.1, for systematic evaluation of the dam seismic behavior so that a combination of all previously defined criteria in conjunction with *LE* analysis are used in the proposed methodology.

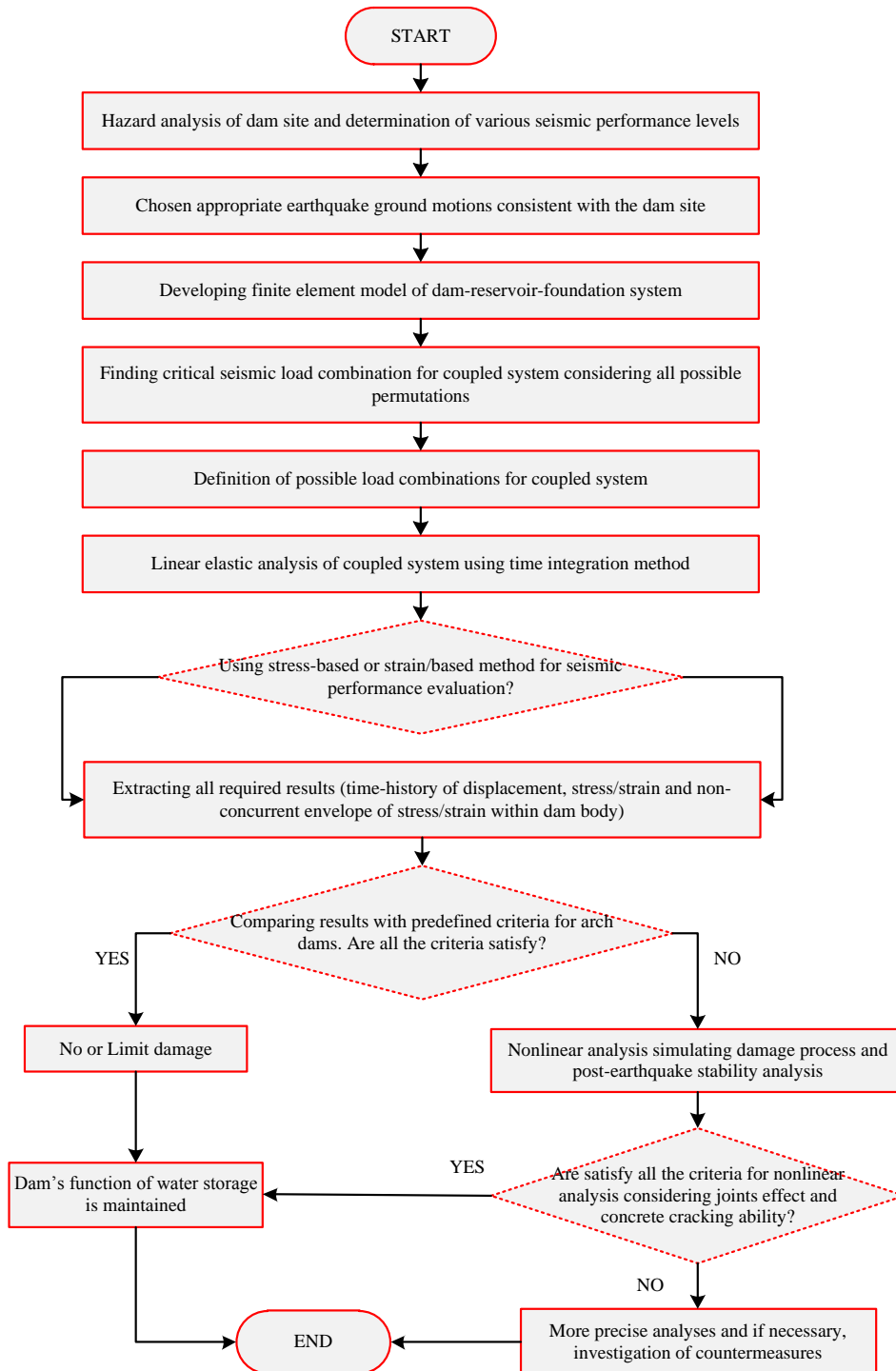


Fig. 2 Flowchart for seismic safety evaluation of arch dams using stress or strain-based indices

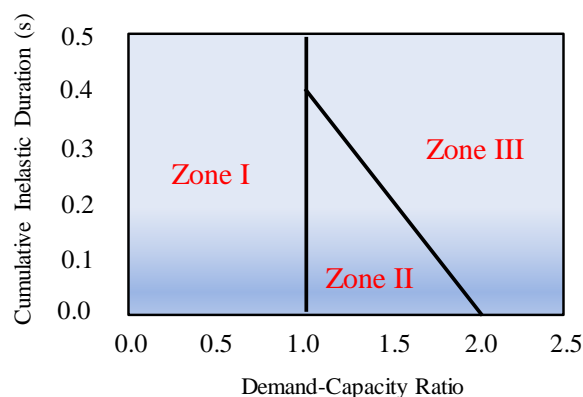


Fig. 3 Zoning the CID-DCR diagram and PTC for arch dams (USACE 2007)

Table 1 Mathematical presentation of the limit-states (USACE 2007)

Limit states	DCR		DCR-CID Diagram		$A^{overstress}$ or $A^{overstrain}$
Minor or No Damage	$DCR \leq 1.0$	&	Zone I	&	0.0%
Acceptable Level of Damage	$1.0 < DCR < 2.0$	&	Zone II	&	$\leq 20.0\%$
Severe Damage	$DCR \geq 2.0$	or	Zone III	or	$> 20.0\%$

3. Dam-water-foundation rock system

One of the main aspects in the seismic loading and wave propagation within the semi-infinite medium such as rock underlying structures is preventing the wave reflection from the artificial boundary of the infinite medium in the finite element analysis. In the present paper the infinite elements method is used for modeling the far-end boundary of the foundation. Using the infinite elements, the stiffness and the damping pertinent to the semi-infinite medium via the artificial boundary of the structure are accounted for in the analyses. The basic idea in utilizing infinite elements is to use the elements with the special shape functions for the geometry at the far-end truncated boundary. Therefore, there will be two sets of shape functions, the standard shape function, N_i , and a growth shape function, M_i . The growth shape function, M_i , grows without limit as the coordinate of i^{th} node approaches infinity, and is applied to the geometry (Mirzabozorg *et al.* 2012). The growth shape functions, M_i , and their derivatives are presented in Table 2 for a twenty-node solid element with a face in the infinity (Fig. 5).

In order to obtain accurate responses of dam under dynamic loads it is required that an appropriate formulation is governed for fluid-structure interaction (FSI) problem and suitable boundary conditions are defined for reservoir medium. Hydrodynamic pressure distribution in reservoir is governed by the pressure wave equation. Assuming that water is linearly compressible and neglecting viscosity, small-amplitude ir-rotational motion of water is governed by Helmholtz equation given as (Seyedpoor *et al.* 2011)

$$\nabla^2 p(x, y, z) = \frac{1}{C_0^2} \ddot{p}(x, y, z, t) \quad (3)$$

where p is hydrodynamic pressure and C_0 is velocity of pressure wave in water. The boundary conditions required for solving the above differential equation is given in Fig. 4. In addition, it represents the coupled equations governing the dynamic behavior of the structure and the reservoir. Finally the equation of motion for dam-reservoir-foundation coupled system can be solved as explained by Mirzabozorg *et al.* (2012).

Table 2 Growth shape functions and their derivatives for a twenty-node element

Node	M_i	$\partial M_i / \partial \xi$	$\partial M_i / \partial \eta$	$\partial M_i / \partial \zeta$
1	$\frac{(1-\eta)(1-\zeta)(2+\xi+\eta+\zeta)}{2(1-\xi)}$	$\frac{-(1-\eta)(1-\zeta)(3+\eta+\zeta)}{2(1-\xi)^2}$	$\frac{(1-\zeta)(1+\xi+2\eta+\zeta)}{2(1-\xi)}$	$\frac{(1-\eta)(1+\xi+\eta+2\zeta)}{2(1-\xi)}$
2	$\frac{(1+\xi)(1-\eta)(1-\zeta)}{4(1-\xi)}$	$\frac{(1-\eta)(1-\zeta)}{4(1-\xi)^2}$	$\frac{-(1+\xi)(1-\zeta)}{4(1-\xi)}$	$\frac{-(1+\xi)(1-\eta)}{4(1-\xi)}$
6	$\frac{(1+\xi)(1+\eta)(1-\zeta)}{4(1-\xi)}$	$\frac{(1+\eta)(1-\zeta)}{4(1-\xi)^2}$	$\frac{(1+\xi)(1-\zeta)}{4(1-\xi)}$	$\frac{-(1+\xi)(1+\eta)}{4(1-\xi)}$
7	$\frac{(1+\eta)(1-\zeta)(2+\xi+\eta+\zeta)}{2(1-\xi)}$	$\frac{-(1+\eta)(1-\zeta)(3-\eta+\zeta)}{2(1-\xi)^2}$	$\frac{-(1-\zeta)(1+\xi+2\eta+\zeta)}{2(1-\xi)}$	$\frac{(1+\eta)(1+\xi+\eta+2\zeta)}{2(1-\xi)}$
8	$\frac{(1-\xi)(1+\eta)(1-\zeta)}{(1-\xi)}$	$\frac{(1-\eta)(1+\eta)(1-\zeta)}{(1-\xi)^2}$	$\frac{-2\eta(1-\zeta)}{2(1-\xi)}$	$\frac{-(1-\eta)(1+\eta)}{(1-\xi)}$
9	$\frac{(1-\eta)(1-\zeta)(1+\zeta)}{(1-\xi)}$	$\frac{(1-\eta)(1-\zeta)(1+\zeta)}{(1-\xi)^2}$	$\frac{-(1-\zeta)(1+\zeta)}{(1-\xi)}$	$\frac{-2\zeta(1-\eta)}{(1-\xi)}$
12	$\frac{(1+\eta)(1-\zeta)(1+\zeta)}{(1-\xi)}$	$\frac{(1+\eta)(1-\zeta)(1+\zeta)}{(1-\xi)^2}$	$\frac{(1-\zeta)(1+\zeta)}{(1-\xi)}$	$\frac{-2\zeta(1+\eta)}{(1-\xi)}$
13	$\frac{(1-\eta)(1+\zeta)(-2-\xi-\eta+\zeta)}{2(1-\xi)}$	$\frac{(1-\eta)(1+\zeta)(-3-\eta+\zeta)}{2(1-\xi)^2}$	$\frac{-(1+\xi)(-1-\xi+2\eta+\zeta)}{2(1-\xi)}$	$\frac{(1-\eta)(-1-\xi-\eta+2\zeta)}{2(1-\xi)}$
14	$\frac{(1+\xi)(1-\eta)(1-\zeta)}{(1-\xi)}$	$\frac{(1-\eta)(1+\zeta)}{4(1-\xi)^2}$	$\frac{-(1+\xi)(1+\zeta)}{4(1-\xi)}$	$\frac{(1+\xi)(1-\eta)}{4(1-\xi)}$
18	$\frac{(1+\xi)(1+\eta)(1+\zeta)}{4(1-\xi)}$	$\frac{(1+\eta)(1+\zeta)}{4(1-\xi)^2}$	$\frac{(1+\xi)(1+\zeta)}{4(1-\xi)}$	$\frac{(1+\xi)(1+\eta)}{4(1-\xi)}$
19	$\frac{(1+\eta)(1+\zeta)(-2-\xi+\eta+\zeta)}{2(1-\xi)}$	$\frac{(1-\eta)(1+\zeta)(-3+\eta+\zeta)}{2(1-\xi)^2}$	$\frac{-(1+\xi)(-1-\xi+2\eta+\zeta)}{2(1-\xi)}$	$\frac{(1+\eta)(-1-\xi+\eta+2\zeta)}{2(1-\xi)}$
20	$\frac{(1-\eta)(1+\eta)(1+\zeta)}{(1-\xi)}$	$\frac{(1-\eta)(1+\eta)(1+\zeta)}{(1-\xi)^2}$	$\frac{-2\eta(1+\zeta)}{(1-\xi)}$	$\frac{(1-\eta)(1+\eta)}{(1-\xi)}$

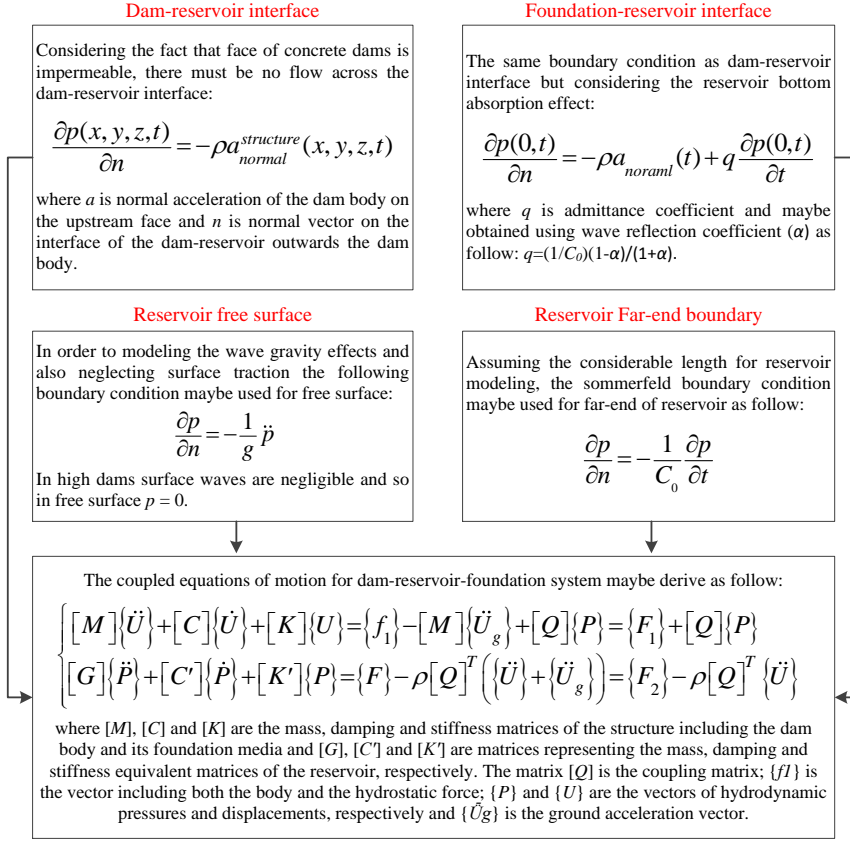


Fig. 4 Mathematical definition of reservoir various boundary conditions and FSI equation of motion

4. Damage mechanics for mass concrete

In order to analysis of a structural system utilizing the damage mechanics approach, the proposed method should be able to simulate the behavior of the element in different states as follow; Pre-softening behavior, fracture energy conservation, nonlinear behavior during the softening phase and finally crack closing/reopening behavior. In the general, the pre-softening behavior of mass concrete is simulated using the Hooke's law considering the linear elastic relationship of the stress and strain vectors. In the present model, the uniaxial strain energy (the area under the stress-strain curve up to the peak stress point or apparent tensile stress) is used as softening initiation criterion. The crack initiates when uniaxial strain energy density, $(\sigma_1 \varepsilon_1 / 2)$, is greater than U_0 in static conditions

$$U_0 = \int_0^{\varepsilon_t} \sigma d_\varepsilon = \frac{\sigma_i \varepsilon_i}{2} \quad (4)$$

Fig. 4 Mathematical definition of reservoir various boundary conditions and FSI equation of motion where σ_i and ε_i are the apparent tensile strength and its corresponding strain, respectively. Considering that the properties of material changes under dynamic loads, the strain rate effect under dynamic loads is applied on the crack initiation criterion as follow

$$U'_0 = \frac{\sigma'^2}{E} = (DMF_e)^2 \times U_0 \quad (5)$$

where DMF_e is dynamic magnification factor and the parameters with the prime sign indicate properties in dynamic condition.

During the softening phase the elastic stress-strain relationship is replaced using the damaged modulus matrix in each of the three principal directions. In the present paper, the secant modulus stiffness (SMS) approach is used for the stiffness matrix formulation. Considering the energy equivalence principle and neglecting the coupling between the three principal fracture modes, the damaged modulus matrix is given as

$$[D]_d = \begin{bmatrix} [D]_d^t & 0 \\ 0 & [D]_d^r \end{bmatrix} \quad (6)$$

where

$$[D]_d^t = \frac{E}{(1+\nu)(1-2\nu)} \begin{bmatrix} (1-\nu)(1-d_1)^2 & & sym. \\ \nu(1-d_1)(1-d_2) & (1-\nu)(1-d_2)^2 & \\ \nu(1-d_1)(1-d_3) & \nu(1-d_2)(1-d_3)(1-\nu)(1-d_3)^2 & \end{bmatrix} \quad (7)$$

$$[D]_d^r = G \begin{bmatrix} \frac{2(1-d_1)^2(1-d_2)^2}{(1-d_1)^2 + (1-d_2)^2} & & sym. \\ 0 & \frac{2(1-d_2)^2(1-d_3)^2}{(1-d_2)^2 + (1-d_3)^2} & \\ 0 & 0 & \frac{2(1-d_1)^2(1-d_3)^2}{(1-d_1)^2 + (1-d_3)^2} \end{bmatrix} \quad (8)$$

where d_1 , d_2 and d_3 are the damage variables corresponding to the principal strains in the local directions. Satisfying the principle of energy equivalence and assuming the linear stress-strain curve in the post-peak phase, d_i is given as

$$d_i = 1 - \sqrt{\frac{\varepsilon_0}{\varepsilon_i} \left(1 - \left(\frac{\varepsilon_i - \varepsilon_0}{\varepsilon_f - \varepsilon_0} \right) \right)} \quad (9)$$

where ε_0 and ε_f are the strains corresponding to the crack initiation and no resistance strain, respectively and ε_i is the principal strain of the element in the considered direction. The proposed modulus matrix includes all of the principal fracture modes. However, as mentioned, in the proposed formulation, the interaction between the three principal fracture modes and mixed modes is neglected.

The damaged modulus matrix shown in Eq. (6) is in the local coordinate which is corresponding to the direction of the principal strains. This matrix should be transformed to the global coordinate as following

$$[D]_s = [T]^T [D]_d [T] \quad (10)$$

where, $[T]$ is the strain transformation matrix. Based on the maximum strain reached in each principal direction, the secant modulus matrix is determined. Clearly, increasing of the strain leads to increasing the corresponding damage variable and finally, when the strain reaches to the fracture strain, the element is fully cracked in the corresponding direction and the related damage variable sets to be unit. In fact, any change in the principal strain or its direction leads to update requirement of the global constitutive matrix, $[D]_s$. Satisfying the fracture energy conservation principle in the static and the dynamic loading conditions, the no resistance strain is given as

$$\varepsilon_f = \frac{2G_f}{\sigma_0 h_c}, \quad \varepsilon'_f = \frac{2G'_f}{\sigma'_0 h_c} \quad (11)$$

where, h_c is the characteristic dimension of the cracked Gaussian point and is assumed equal to the third root of the Gaussian point's contribution volume within the cracked element. The primed quantities show the dynamic constitutive parameters. The strain-rate sensitivity of the specific fracture energy is taken into account through the dynamic magnification factor DMF_f as follows

$$G'_f = DMF_f \times G_f \quad (12)$$

It is worth noting that DMF_f is mainly contributed by DMF_e . In the current formulation, Co-axial Rotating Crack Model (CRCM) is used to simulation of the cracked Gaussian point's behavior within the cracked elements. In this approach shear stiffness factors (arrays of matrix in Eq. (8)) are determined based on the state of the Gaussian point in each principal direction in the current time step. As softening within the considered element progresses, the shear stiffness factor in the cracked Gaussian point decreases corresponding to the state of the principle strains and may reach to zero value and therefore, the constitutive matrices contributions of the cracked Gaussian point and finally, the constitutive matrix of the considered element must be updated as these factors are changed (Mirzabozorg *et al.* 2004).

Under the cyclic loading, there is residual strain in the closed Gaussian point. This concept has been used in the element level approaches in which the total strain in each Gaussian point is decomposed into the two components of the elastic and the residual strain given as Ardakanian *et al.* (2006)

$$\varepsilon = \varepsilon^e + \varepsilon^{in} = \varepsilon^e + \lambda \varepsilon_{\max} \quad (13)$$

where ε_{max} is the maximum principal strain which the Gaussian point has reached during the previous cycles and λ is the ratio between the residual strain in the closed Gaussian point and the maximum principal strain and is normally given as 0.2.

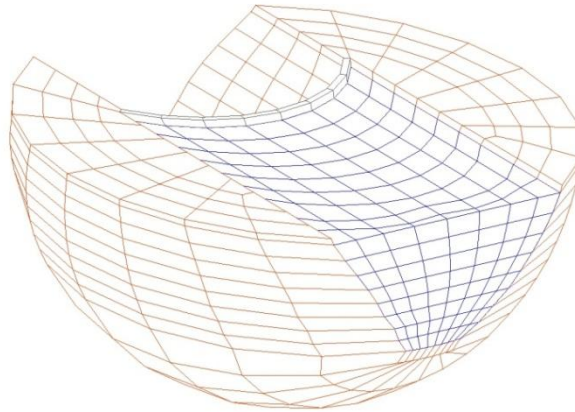


Fig. 5 Finite element model of dam-reservoir-massed foundation system of *Karadj* Dam

5. Numerical example

Karadj Dam is 168 m double curvature arch dam. Its thickness at the crest and the bottom is 7.85m and 32.0m, respectively. Finite element model of the dam-reservoir-foundation system is shown in Fig. 5. Its foundation is modeled as massed media in circular shape and the far-end boundary of the foundation extended to a distance about twice of the dam height in all directions and infinite elements are used on outer boundaries (Mirzabozorg *et al.* 2012). Reservoir is modeled based on Eulerian approach as compressible material and its length is more than the dam height. Eight-node fluid elements with one pressure degree of freedom are used in reservoir domain. Sharan boundary condition is used for far-end of the reservoir to absorb all outgoing waves (Sharan 1986). Sloshing effect of the reservoir water is neglected due to the height of the dam. Moreover, reservoir-dam interaction and reservoir-foundation interaction are considered in this model using implementation of the four-node solid-fluid interface elements (nine Gaussian points). Dam-reservoir-foundation model consists of 1628 twenty-node solid elements for simulation of the dam body and its foundation and 720 eight-node fluid elements for the reservoir domain. Fig. 6 shows all the used elements for modeling the dam body, reservoir, massed foundation and fluid-solid interface elements. Material properties for the mass concrete, foundation rock and the reservoir water are given in Table 3.

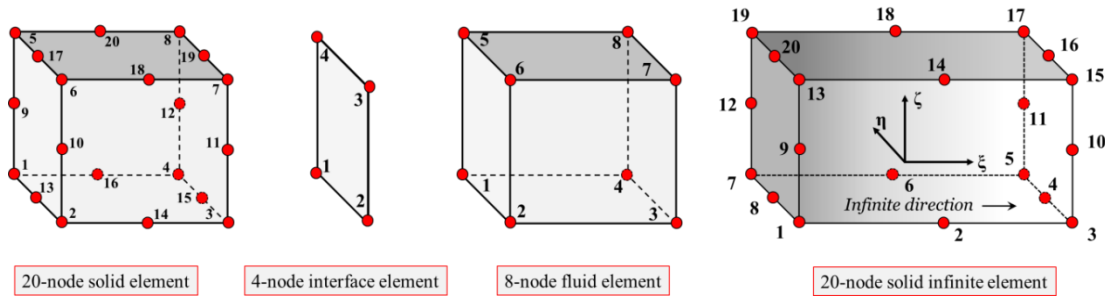


Fig. 6 Finite and infinite elements for modeling coupled system

Table 3 Material properties for *Karadj* Dam

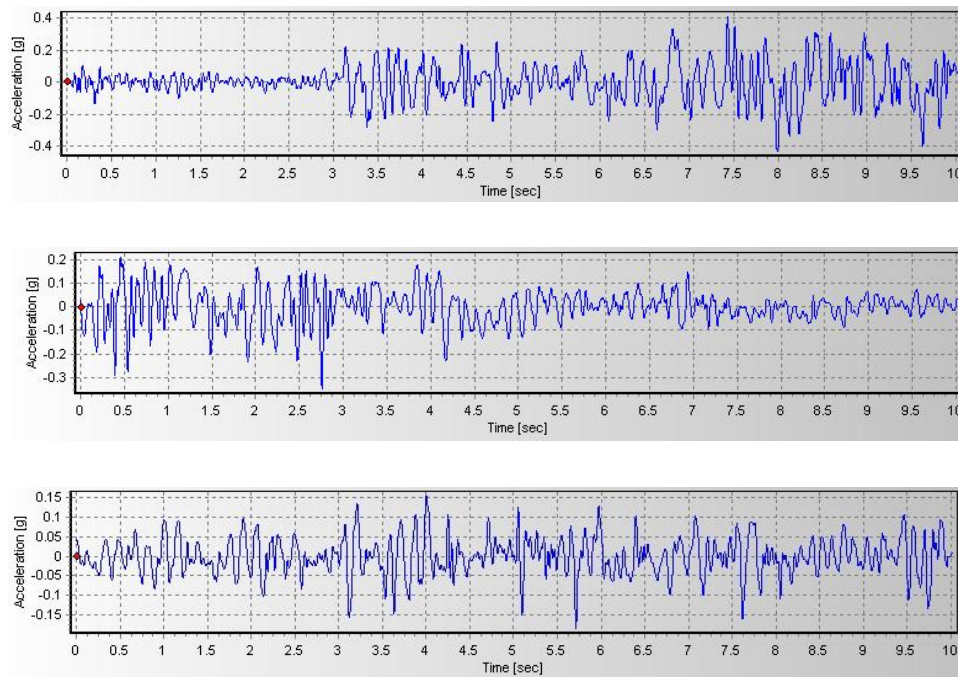
Properties		Static Values	Dynamic Values
	Isotropic Elasticity	26GPa	29.9GPa
	Poisson's Ratio	0.17	0.12
Mass	Mass Density		2450 kg/m ³
Concrete	Uniaxial Compressive Strength	37.9MPa	39.6MPa
	Uniaxial Tensile Strength	3.65MPa	5.47MPa
	Thermal Expansion Coefficient		8e-6 1/°C
Foundation	Deformation Modulus		16.3GPa
	Poisson's Ratio		0.15
Rock	Mass Density		3000 kg/m ³
	Speed of pressure wave		1000kg/m ³
Water	Mass Density		1440m/s
	Wave Reflection Coefficient		0.8

Load combinations corresponding to the summer and winter conditions were used in conjunction with maximum credible earthquakes (*MCE*). The applied loads are the dam body self-weight, hydrostatic pressure, thermal loads obtained from thermal transient analysis of dam and finally seismic loads based on the considered seismic performance level. The load combination of *Karadj* dam can be summarized as:

- a) Load Combo W-MCE00: W (dam self-weight) + h_s (hydrostatic pressure) at *MWL* (minimum water level) + T_w (winter temperature) + *MCE* (maximum credible earthquakes)

- b) Load Combo S-MCE00: W (dam self-weight) + h_s (hydrostatic pressure) at NWL (normal water level) + T_s (summer temperature) + MCE (maximum credible earthquakes)

In each case, the load combination is shown with an abbreviation in which the first letter represents thermal/hydrostatic load condition, the other letters are the type of the seismic load and the final two numbers represents No. of earthquake ground motion. It is noteworthy that three ground motions were selected for seismic analyses based on source characteristics, source-to-site transmission path properties, and site conditions (USACE 2003 and USACE 2007). These ground motions are 1990 Rudbar (at *Tabas* station) as No.01, 1994 Northridge (at *Moorpark-fire* station) as No.02 and 1952 Taft Lincoln (at *Taft Lincoln* school station) as No.03. Time history of these ground motions are depicted in Fig. 7.



(a)

Continued

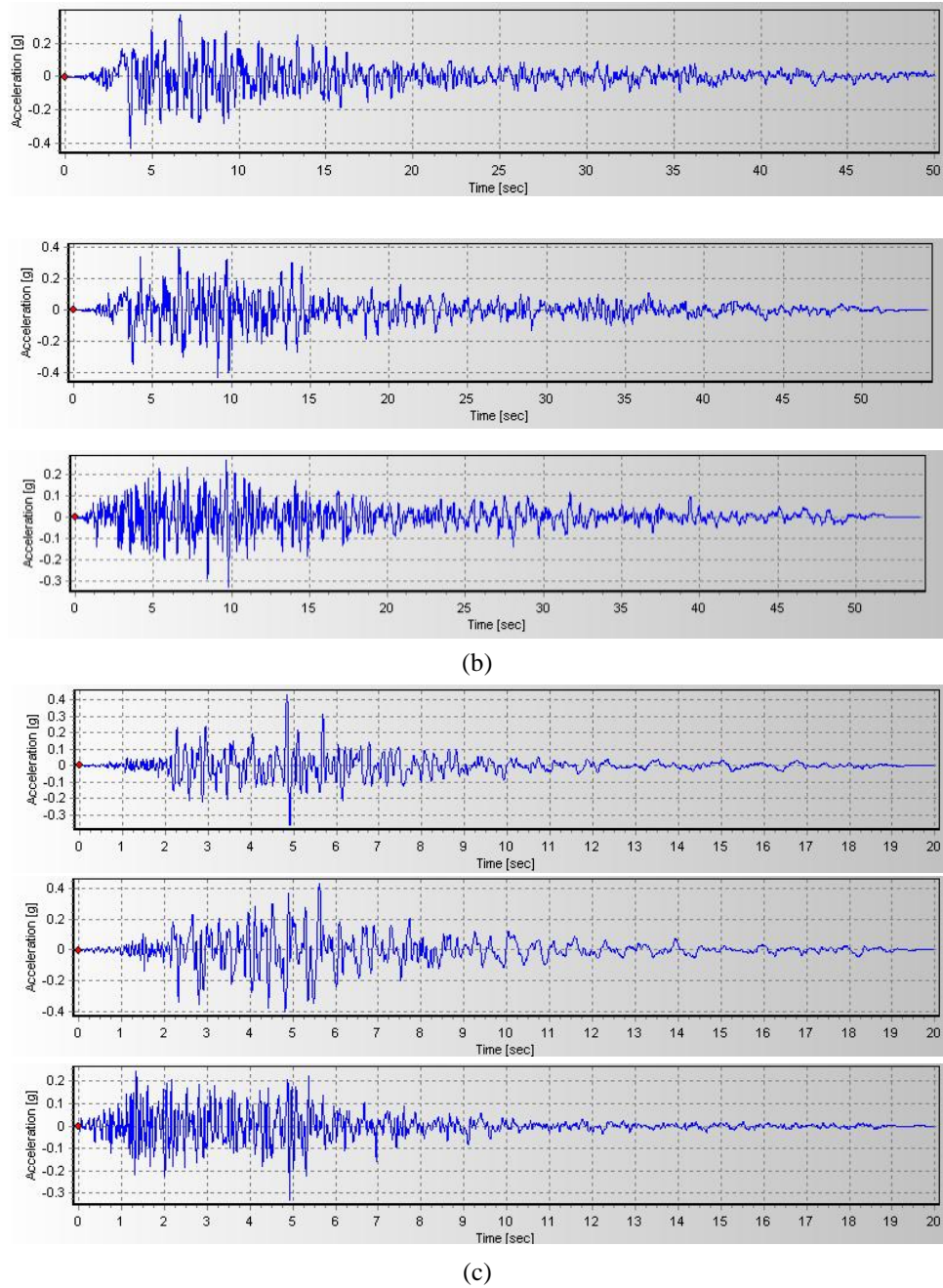


Fig. 7 Time history of ground motions in stream, cross-stream and vertical directions: (a) Rudbar, (b) Taft Lincoln and (c) Northridge

All ground motions are scaled based on horizontal and vertical components of acceleration response spectrums in various excitation levels. The acceleration response spectrums for *Karadj* dam was extracted considering $\xi=5\%$ as shown in Fig. 8. The *Newmark- β* time integration method is utilized to solve the coupled equation of motions (Mirzabozorg and Ghaemian 2005). The system is excited at the foundation boundaries using aforementioned earthquake records. Moreover structural damping is taken to be 5% of critical damping.

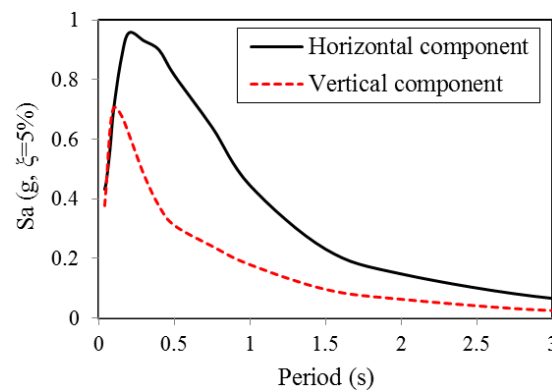


Fig. 8 Acceleration response spectrums of *Karadj* dam in *MCL*

In addition thermal loads considering the summer and winter conditions are applied in models. Thermal loads are obtained from thermal transient analysis of the dam considering water temperature, air temperature and solar radiation in the dam site (Sheibani and Ghaemian 2001). The used temperatures on the US and DS faces of the dam body are shown in Fig. 9.

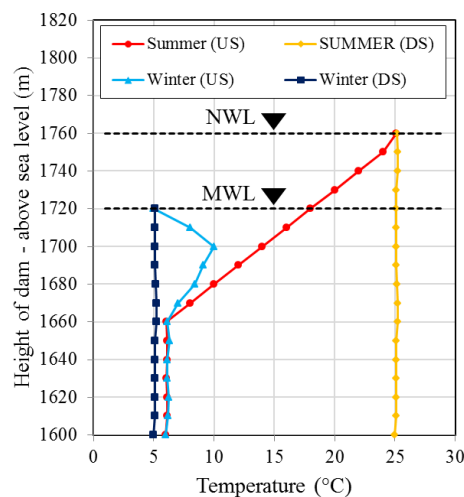


Fig. 9 Temperatures distribution in upstream and downstream faces of dam

6. Results and discussion

In this section, the results of the linear analysis of *Karadj* Dam are discussed based on the stress and strain indices and compared with the real crack profiles resulted from nonlinear analyses. For analysis of coupled dam-reservoir-foundation system the NSAD-DRI finite element code was used (Mirzabozorg *et al.* 2012).

6.1. Arch actions

Fig. 10 shows the time-history of the arch stress or strain at the most critical node in the dam body. As can be seen, although the general trends of the stress and strain are close in all cases, there are some differences between them. For example in W-MCE01 load combination, the time at which the first cycle of arch stress exceeds $DCR=1$ is 6.08s while the first arch strain cycle over the $DCR=1$ is in $t=7.01$ s. So the dam body (and in fact the dam blocks) experiences strain-based damage 0.97s after stress-based damage. In the other word, contraction joints remain in complete close status about one second in strain-based method more than the stress-based evaluation. The total number of cycles that the critical node exceeds from $DCR=1$ in stress-based and strain-based indices are 130 and 120, respectively. In addition, the maximum DCR value for the stress-based index and the strain-based index are 2.08 and 1.92 respectively, which shows the critical condition in the stress-based index.

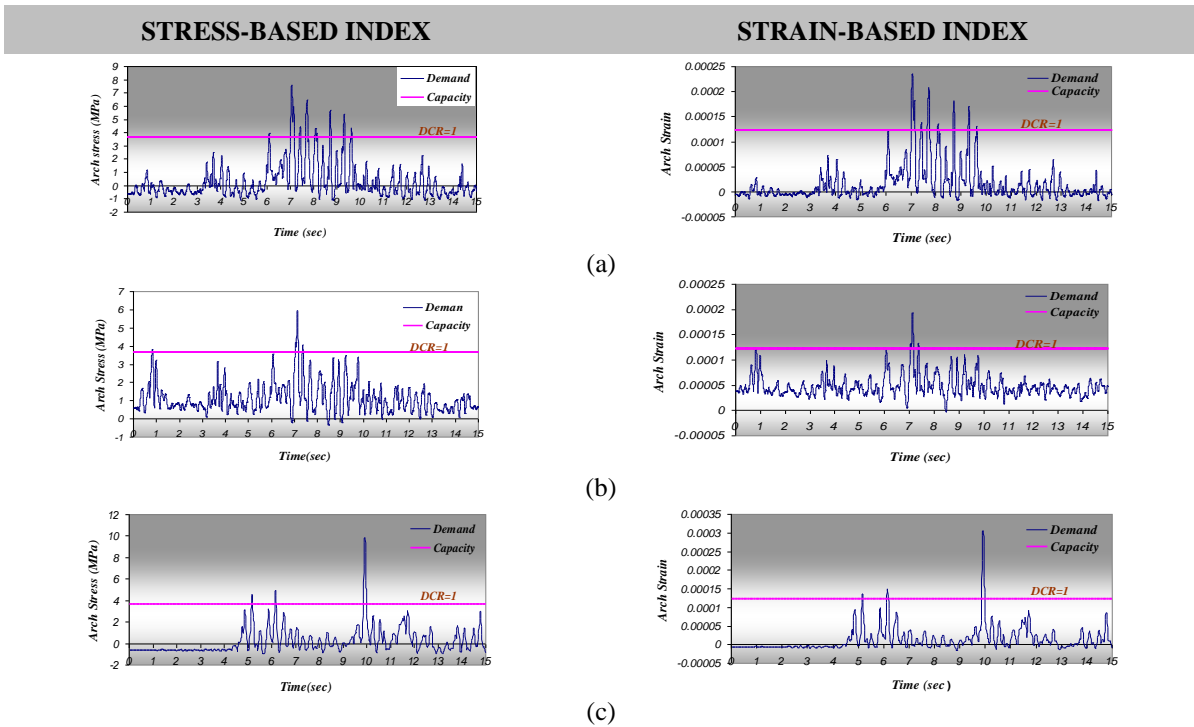
Also, Fig. 11 shows the locations of the critical nodes on both the US and DS faces of the dam body under various load combinations. The critical nodes under W-MCE01 and S-MCE01 are concentrated in upper parts of the dam in vicinity of the crest while in W-MCE02 no probable damage is shown on the US face. Using W-MCE03 and S-MCE03 as seismic input increase the number of critical nodes on both faces and also shift them a bit from center to the sides. Fig. 12 summarizes performance curves for both arch stress and strain as well. As it is clear, almost in all cases summer load combination leads to lower value of cumulative inelastic duration (and also lower performance curve) than the winter load combination. Using strain-based indices leads to generation of performance curve with lower values than stress-based indices. Also, considering the mean performance curve in both cases and comparing them with PTC in Fig. 3, it can be found that based on the stress-based index the mean curve exceeds PTC considerably and so this dam needs to be analyzed taking into account nonlinear properties of mass concrete while based on strain-based index the mean curve is almost coincident with PTC and utilizing some engineering judgment maybe is enough in this case for seismic safety assessment of the dam.

6.2. Cantilever actions

Fig. 13 shows the time-history of the cantilever stress or strain for the most critical node in the dam body. Like as the arch stress or strain, cantilever stress and strain show similar general trend with some small differences. For example, in S-MCE03 load combination, the time at which the first cycle of cantilever stress exceeds $DCR=1$ is 5.87s while the first cantilever strain cycle over the $DCR=1$ is in $t=6.84$ s. So, the dam body experiences strain-based damage 0.97s after the stress-based damage. It means that the lift joints may be opened one second later (if we assume isotropic material property for the mass concrete) under this load combination using strain-based index instead of stress-based index. The total number of cycles that the critical node exceeds from $DCR=1$ in stress-based and strain-based indices are 34 and 17, respectively. The maximum values

of DCR for stress- and strain-based indices are 1.28 and 1.12, respectively which shows the critical condition in stress-based index.

Fig. 14 shows the locations of critical nodes based on cantilever stress or strain in the dam body under various load combinations. Based on this figure, operating the dam under winter load combination is more critical than the summer condition considering cantilever stress or strain as safety index. In spite of the arch stress or strain in which all critical nodes were in upper part of the dam in vicinity of the center, in this case critical nodes are concentrated in middle part of the dam body near the abutments. It shows almost high tensile cantilever stress or strain at the dam-foundation interface. On the other hand, comparing the number of critical nodes on both the US and DS faces reveals that due to cantilever action of blocks and also hydrodynamic pressure effects, US face is exposed to higher tensile stress than the DS face. Fig. 15 summarizes performance curves for the most critical point on the cantilever stress and strain. In all cases, summer load combinations lead to lower value of cumulative inelastic duration and also lower performance curve than the winter load combinations. In addition, there is no performance curve for some of load combinations because the dam experiences no cantilever stress more than the tensile strength of concrete in these cases. Comparing mean performance curve due to stress-based and strain-based indices shows that in both cases they don't exceed performance threshold curve while using strain-based index give more conservative results. So it means that considering cantilever stress or strain as damage index, dam doesn't need to be analyzed utilizing nonlinear constitutive laws.



Continued

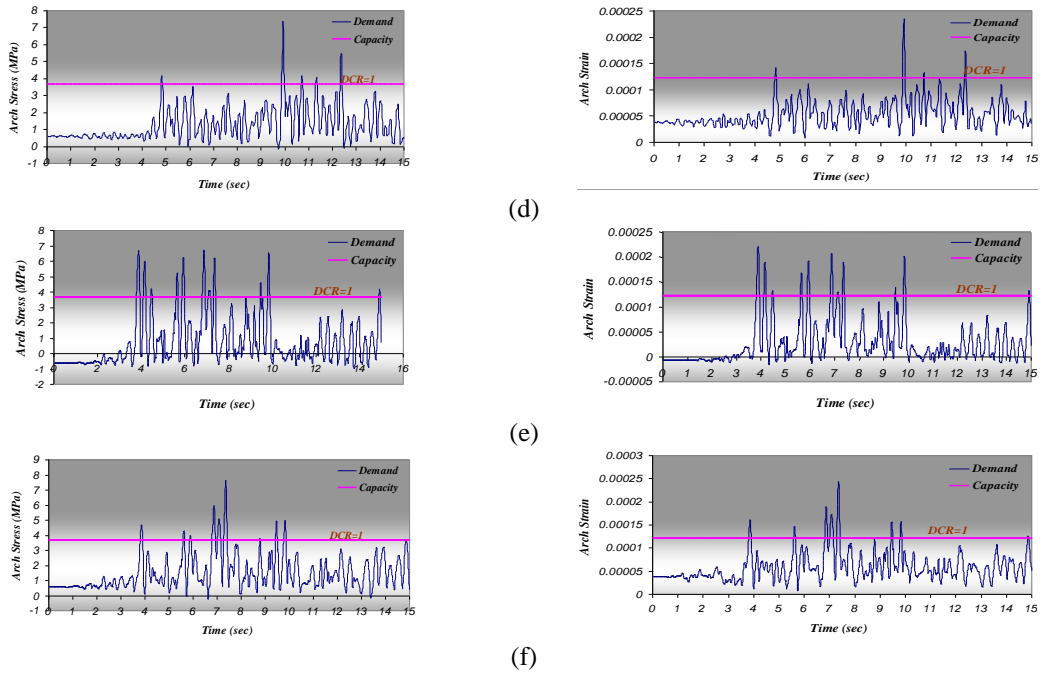


Fig. 10 Time-history of arch stress or strain for most critical node in dam, (a) W-MCE01, (b) S-MCE01, (c) W-MCE02, (d) S-MCE02, (e) W-MCE03 and (f) S-MCE03

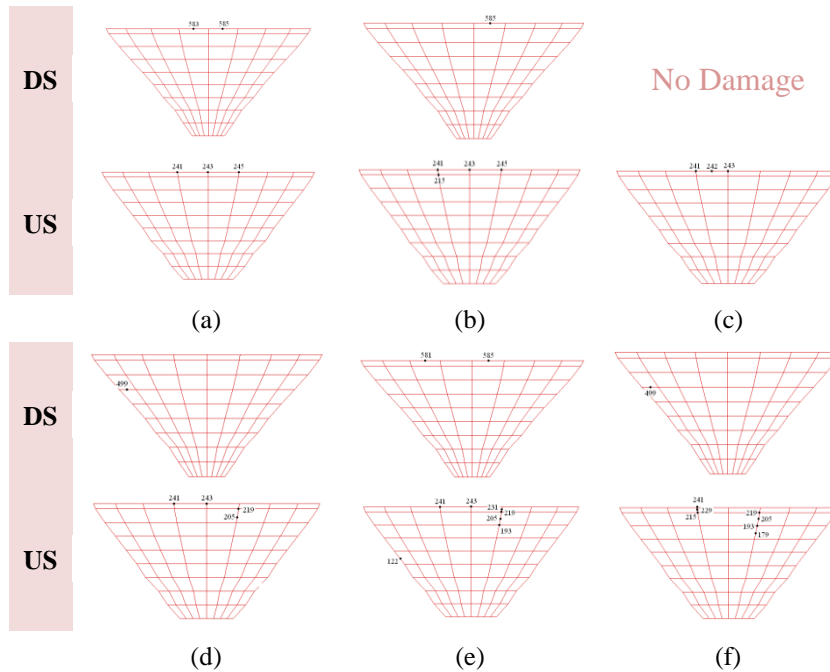


Fig. 11 Locations of critical arch stress or strain in upstream and downstream face, (a) W-MCE01, (b) S-MCE01, (c) W-MCE02, (d) S-MCE02, (e) W-MCE03 and (f) S-MCE03

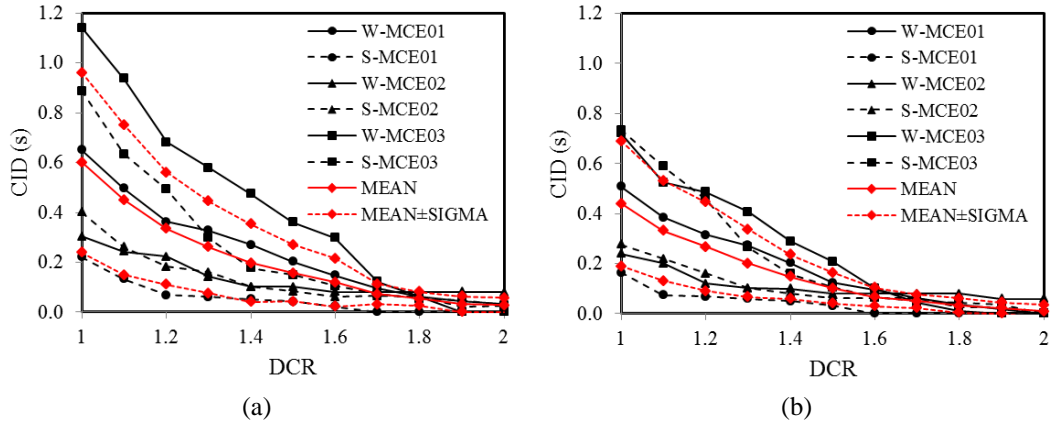
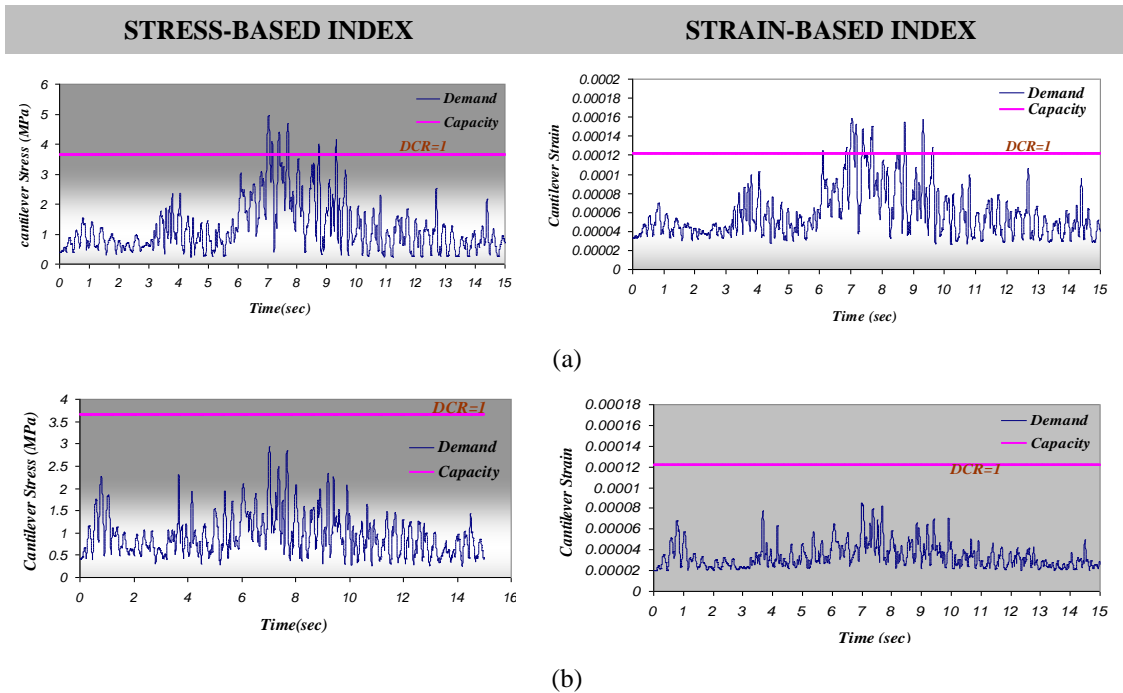
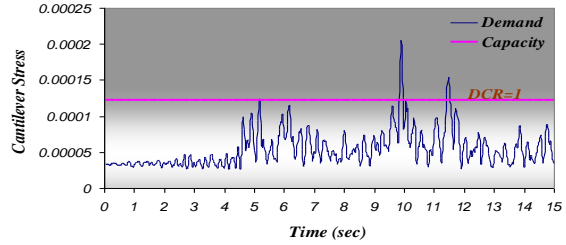
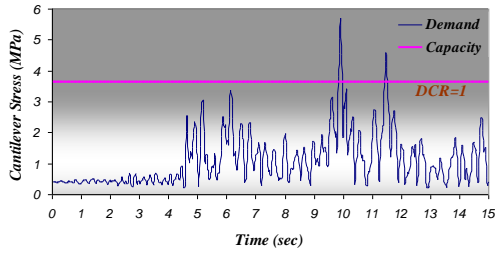


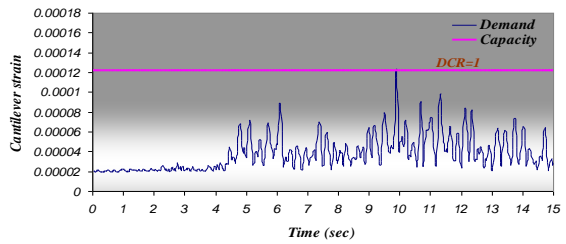
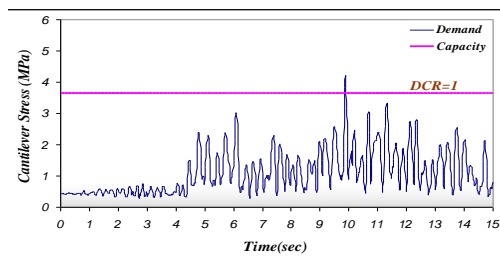
Fig. 12 Performance curves for critical nodes using different load combinations (a) Based on arch stress and (b) Based on arch stain



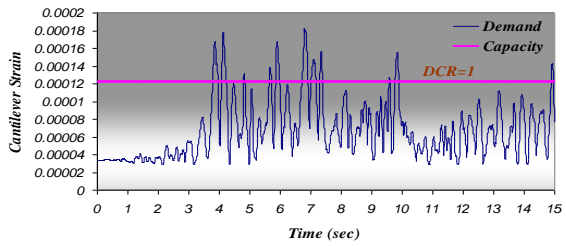
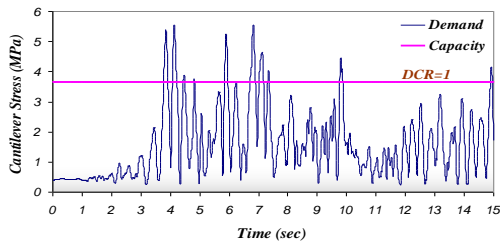
Continued



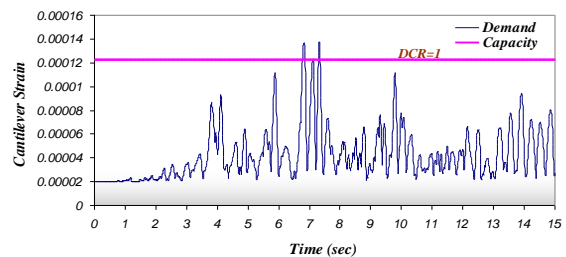
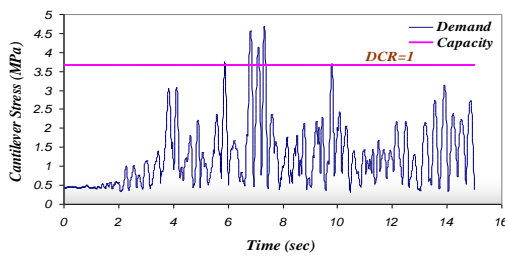
(c)



(d)



(e)



(f)

Fig. 13 Time-history of cantilever stress or strain for most critical node in dam, (a) W-MCE01, (b) S-MCE01, (c) W-MCE02, (d) S-MCE02, (e) W-MCE03 and (f) S-MCE03

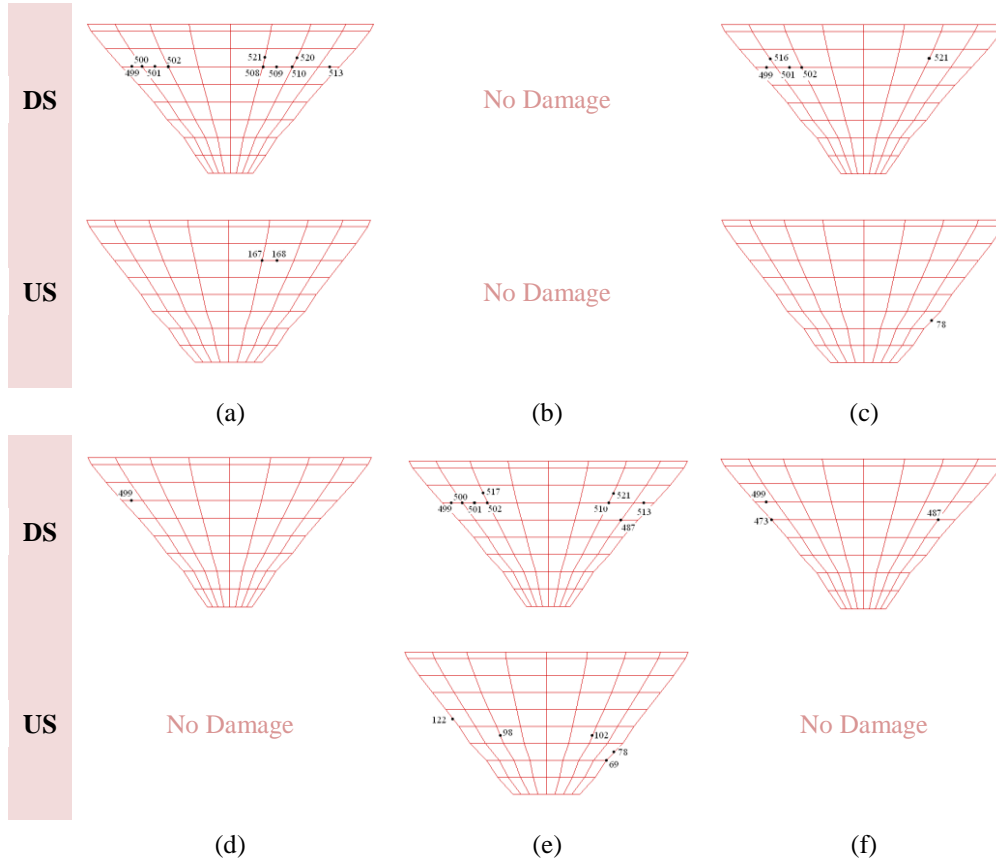


Fig. 14 Locations of critical cantilever stress or strain in upstream and downstream face, (a) W-MCE01, (b) S-MCE01, (c) W-MCE02, (d) S-MCE02, (e) W-MCE03 and (f) S-MCE03

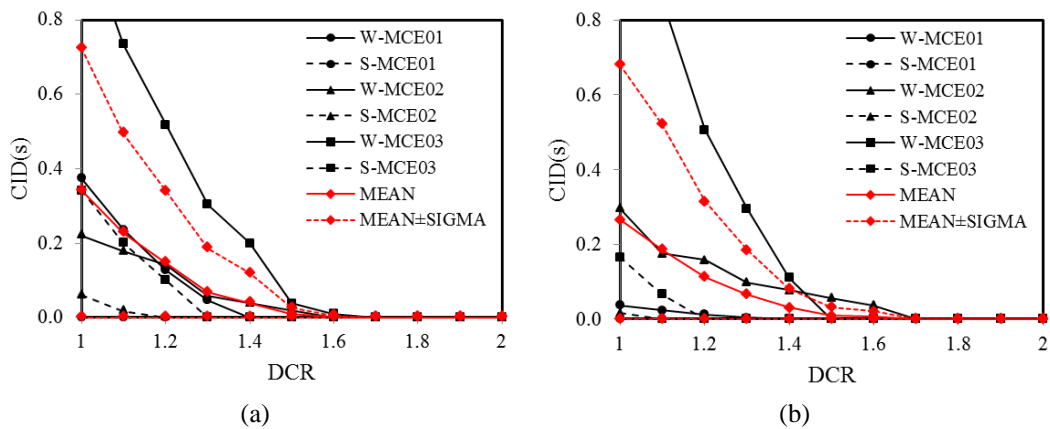


Fig. 15 Performance curves for critical nodes using different load combinations (a) based on cantilever stress and (b) based on cantilever strain

6.3. Linear vs. nonlinear analyses

In order to validate the results of the seismic performance evaluation of the arch dams based on stress and strain approaches, the results of the overstrained regions at different level of performance is compared with the real crack profile obtained from the nonlinear damage analysis of the coupled system. The cracking profile is extracted based on damage mechanics approach and is represented in the form of the Cracked Gaussian Points (CGPs) in upstream and downstream faces of the dam body.

Fig. 16 compares the results of the estimated and real crack profiles for different load combinations. In all cases the real crack profile on the dam is compared with overstrained regions obtained based on the maximum arch and cantilever strains. It should be mentioned that based on the theory of the damage mechanics for the concrete, explained in section 4, the strain-based approach in principal strain domain is used also in order to figure out the cracked Gaussian points. DCR for different values were calculated and plotted as counter on the dam (the red-line counter shows the regions with DCR more than one which has theoretically high capability for cracking).

As can be seen almost in all cases the overstrained regions estimated based in the arch and cantilever strains are in good agreement with those obtained from nonlinear damage analysis of the dam. Due to the nature of nonlinear analysis and updating the elements properties in each load step, it's not expected that the location of the cracked point be exactly as same as the linear model; however, the general patterns of the estimated crack profiles using the strain-based method are very close to real crack profile. In all cases the results of the nonlinear damage analysis cover the sum of the overstrained regions by arch and cantilever strains.

7. Conclusions

Currently, all guides on seismic assessment of dams are using/proposing the stress-based criteria for evaluation of mass concrete behavior under dynamic loading while cracking nature of the concrete is originally based on strain criteria. In the present paper, the seismic performance assessment of an arch dam was investigated using the criteria based on both the stress and the strain. For this purpose *Karadj* Dam was selected and the numerical model of the dam-reservoir-massed foundation was provided using the finite element technique. Two different load combinations were considered as winter and summer as well as three various ground motions in *MCL* for each of them.

For the arch actions, almost in all cases, summer load combinations lead to lower value of cumulative inelastic duration and also lower performance curve than the winter load combinations. Using strain-based indices leads to generation of the performance curve with lower values than stress-based indices. Also the mean performance curve in stress-based approach exceeds *PTC* considerably while according to the strain-based index the mean curve is almost coincident with *PTC*.

For the cantilever actions, critical nodes are concentrated in middle part of the dam near the abutments. Also, upstream face is exposed to higher tensile cantilever stress than the downstream face. Like the previous one, in all cases, summer load combinations lead to lower value of cumulative inelastic duration and also lower performance curve than the winter load combinations. None of the mean performance curves based on stress and strain approaches are exceed *PTC* while using strain-based index gives more conservative results.

It's important to note that the behavior of mass concrete especially in cracking is based on the strain variation. Also the main performance of the concrete arch dams is their cantilever action because of releasing the tensile arch stresses due to vertical joints. Therefore, utilizing the strain-based criteria leads to more reliable interpretations and decision-making in the dam safety field and should be used for practical design of arch dams. Finally, the estimated overstrained regions are compared with the real crack profile from the nonlinear damage analysis of the dam. The results of the nonlinear analyses satisfy the estimated overstrained regions with acceptable accuracy.

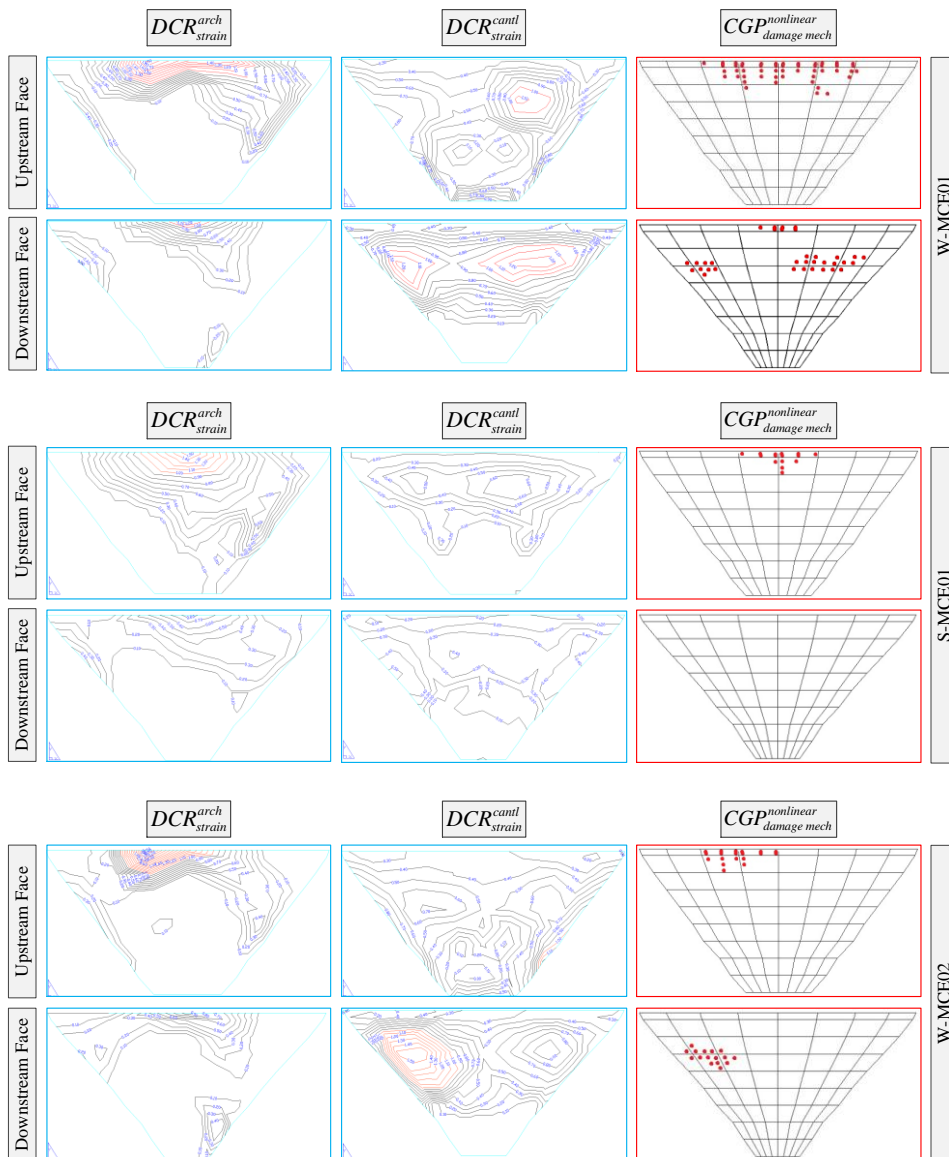


Fig. 16 Comparison of the real crack profile on dam and the estimated overstrained regions(continued)

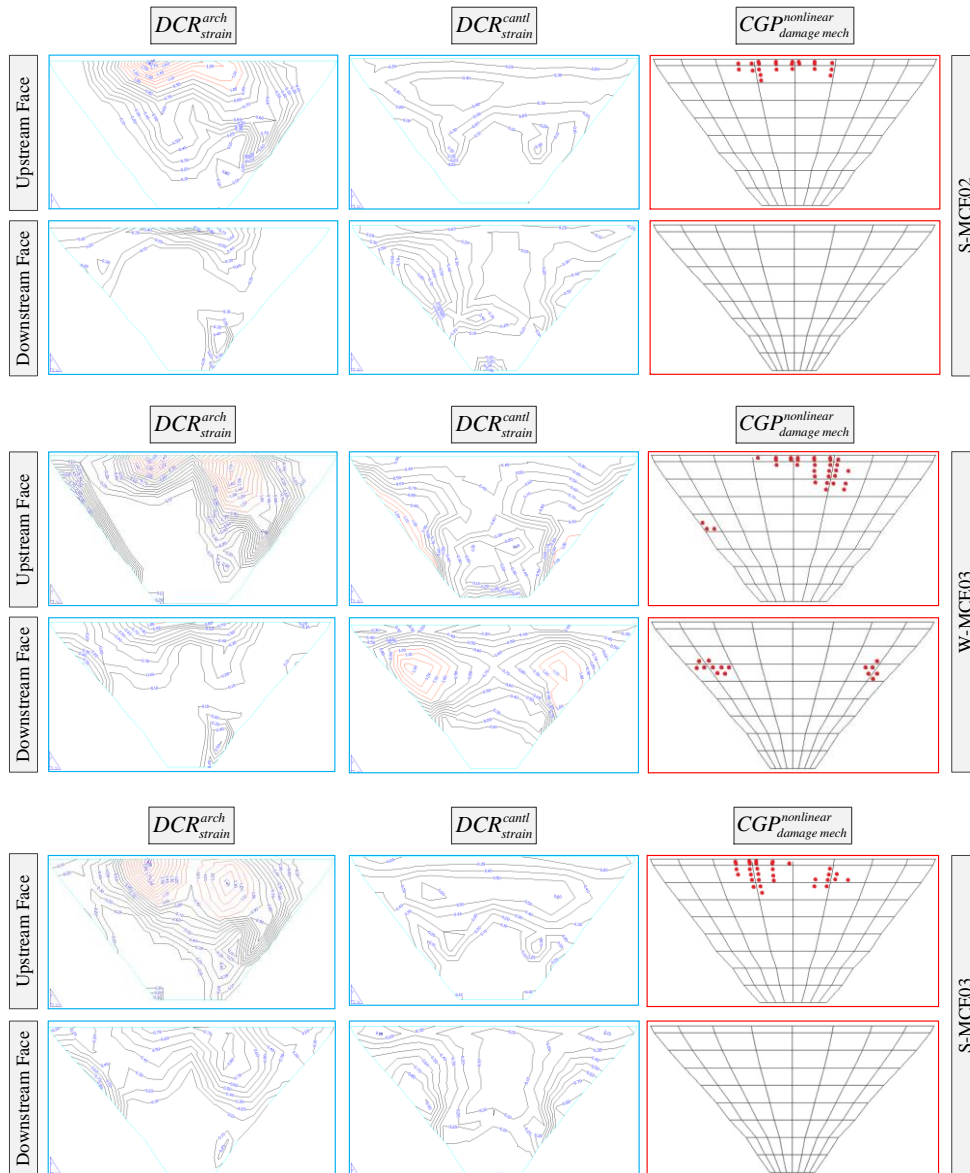


Fig. 16 Comparison of the real crack profile on dam and the estimated overstressed regions

References

- Ardakanian, M., Ghaemian, M. and Mirzabozorg, H. (2006), "Nonlinear behavior of mass concrete in three-dimensional problems using damage mechanics approach", *Int. J. Earthq. Eng. Seismology* (European Earthquake Engineering), **2**, 89-65.

- Bayraktar, A., Sevim, B., Altunisik, A.C., Turker, T., EmreKarta, M., Akkose, M. and Bilici, Y. (2009), "Comparison of near and far fault ground motion effects on the seismic performance evaluation of dam-reservoir-foundation systems", *Dam Eng.*, **19**(4), 201-239.
- Calayir, Y. and Karaton, M. (2005), "A continuum damage concrete model for earthquake analysis of concrete gravity dam-reservoir systems", *Soil Dyn. Earthq. Eng.*, **25**(11), 857-869.
- Chopra, A.K. (1988), *Earthquake response analysis of concrete dams*, (Ed. Jansen, R.B.), Advanced Dam Engineering for Design, Chapter 15: Construction and rehabilitation, New York, NY, USA.
- Ghanaat, Y. (2004), "Failure modes approach to safety evaluation of dams", *Proceedings of the 13th World Conference on Earthquake Engineering*, Vancouver, B.C., Canada.
- Hall, R.L., Matheu, E.E. and Liu, T.C. (1999), "Performance evaluation of the seismic response of concrete gravity dams", *Proceedings of the International Conference on Health Monitoring of Civil Infrastructure Systems*, Chongqing, China, 175-180.
- Hariri-Ardebili, M.A., Mirzabozorg, H. and Ghaemian, M. (2011), "Seismic performance evaluation of high arch dams considering reservoir fluctuation", *Proceeding of the 6th International Conference in Dam Engineering*, Lisbon, Portugal.
- Hariri-Ardebili, M.A. and Mirzabozorg, H. (2011), "Investigation of endurance time method capability in seismic performance evaluation of concrete arch dams", *Dam Eng.*, **22**(1), 35-64.
- Hariri-Ardebili, M.A., Mirzabozorg, H. and Kianoush, R. (2012), "A study on nonlinear behavior and seismic damage assessment of concrete arch dam-reservoir-foundation system using endurance time analysis", *Int. J. Optimiz. Civil Eng.*, **2**(4), 573-606.
- Horii, H. and Chen, S.C. (2003), "Computational fracture analysis of concrete gravity dams by crack-embedded elements-toward an engineering evaluation of seismic safety", *Eng. Fract. Mech.*, **70**(7-8), 1029-1045.
- Mirzabozorg, H. and Ghaemian, M. (2005), "Nonlinear behavior of mass concrete in three-dimensional problems using smeared crack approach", *Earthq. Eng. Struct. D.*, **34**(3), 247-269.
- Mirzabozorg, H., Hariri-Ardebili, M.A. and Nateghi-A., R. (2012), "Seismic behavior of three dimensional concrete rectangular containers including sloshing effects", *J. Coupled Syst. Mech.*, **1**(1), 79-98.
- Mirzabozorg, H., Ghaemian M. and Kianoush, M.R. (2004), "Damage mechanics approach in seismic analysis of concrete gravity dams including dam-reservoir interaction", *Int. J. Earthq. Eng. Seismology* (European Earthquake Engineering), **18**(3), 17-24.
- Mirzabozorg, H., Kordzadeh, A. and Hariri-Ardebili, M.A. (2012), "Seismic response of concrete arch dams including dam-reservoir-foundation interaction using infinite elements", *Electron. J. Struct. Eng.*, **12**(1), 63-73.
- Omidi, O., Valliappan, S. and Lotfi, V. (2013), "Seismic cracking of concrete gravity dams by plastic-damage model using different damping mechanisms", *Finite Elem. Anal. Des.*, **63**, 80-97.
- Oliveira, S. and Faria, R. (2006), "Numerical simulation of collapse scenarios in reduced scale tests of arch dams", *Eng. Struct.*, **28**(10), 1430-1439.
- Pan, J., Zhang, C., Xu, Y. and Jin, F. (2011), "A comparative study of the different procedures for seismic cracking analysis of concrete dams", *Soil Dyn. Earthq. Eng.*, **31**(11), 1594-1606.
- Papadrakakis, M., Papadopoulos, V., Lagaros, N.D., Oliver, J., Huespe, A.E. and Sánchez, P. (2008), "Vulnerability analysis of large concrete dams using the continuum strong discontinuity approach and neural networks", *Struct. Saf.*, **30**(3), 217-235.
- Raphael, J.M. (1984), "The tensile strength of concrete," *ACI Journal Proceedings*, **81**, 158-165.
- Studer, J.A. (2004), "Evaluation of earthquake safety of new and existing dams: Trends and experience", *Proceedings of the 13th World Conference on Earthquake Engineering*, Vancouver, B.C., Canada.
- Seyedpoor, S.M., Salajegheh, J., Salajegheh, E. and Gholizadeh, S. (2011), "Optimal design of arch dams subjected to earthquake loading by a combination of simultaneous perturbation stochastic approximation and particle swarm algorithms", *Appl. Soft Comput.*, **11**(1), 39-48.
- Sharan, S. (1986), "modeling of radiation damping in fluids by finite element", *Int. J. Numer. Meth. Eng.*, **23**, 945-57.
- Sheibani, F. and Ghaemian, M. (2001), "Effects of environmental action on thermal stress analysis of karaj

- concrete arch dam” , *J. Eng. Mech. - ASCE*, **132**(5), 532-544.
- USACE: EM 1110-2-6051, (2003), *Time-history dynamic analysis of concrete hydraulic structures*, US Army Corps of Engineers, Washington, D.C.
- USACE: EM 1110-2-6053, (2007), *Earthquake design and evaluation of concrete hydraulic structures*, US Army Corps of Engineers, Washington, D.C.
- Wieland, M., Brenner R.P. and Sommer, P. (2003), “Earthquake resiliency of large concrete dams: Damage, repair, and strengthening concepts”, *Proceedings of the 21st International Congress on Large Dams*, ICOLD, Montreal, Canada
- Yamaguchi, Y., Hall, R., Sasaki, T., Matheu, E., Kanenawa, K., Chudgar, A. and Yule, D. (2004), “Seismic performance evaluation of concrete gravity dams”, *Proceedings of the 13th World Conference on Earthquake Engineering*, Vancouver, B.C., Canada.
- Zhang, S., Wang, G., Pang, B. and Du, C. (2013), “The effects of strong motion duration on the dynamic response and accumulated damage of concrete gravity dams”, *Soil Dyn. Earthq. Eng.*, **45**, 112-124.